J. Chem. Sci. Vol. 124, No. 4, July 2012, pp. 827–834. © Indian Academy of Sciences.

Synthesis, characterization and investigation of catalytic activity of $Cu_{1-x}Co_xFe_2O_4$ nanocatalysts in *t*-butylation of *p*-cresol

REZA FAREGHI ALAMDARI[a,*], ZAHRA HOSSEINABADI[a] and MASOUD FARHADI KHOUZANI[b]

[a]Faculty of Material and Manufacturing Technologies, Malek Ashtar University of Technology, Tehran 15875-1774, Iran

[b]Institute of Nanoscience and Nanotechnology, University of Kashan, Kashan 87317-51167, Iran

e-mail: reza_fareghi@yahoo.com

MS received 23 April 2011; revised 18 December 2011; accepted 26 December 2011

Abstract. In this work, tertiary butylation of *p*-cresol was carried out in the presence of $Cu_{1-x}Co_xFe_2O_4$ (x = 0 to 1) nanocatalysts by employing methyl-*tert*-butyl ether (MTBE) and *tert*-butyl alcohol (TBA) as alkylation agents. Effects of temperature, mole ratio, type and catalyst composition, time and solvent in reaction conditions were investigated. These nanocatalysts were synthesized using hydrothermal method. The characterization of these catalysts was investigated by means of X-ray diffraction (XRD), Scanning Electron Microscopy (SEM) and Fourier Transform Infrared (FT-IR). These nanocatalysts can be recovered and recycled. A good correlation was found between the activity, in terms of *p*-cresol conversion and various product selectivities for this reaction, and also the acid–base properties of the catalysts. Nano-sized $Cu_{0.5}Co_{0.5}Fe_2O_4$, in comparison to the other nanocatalysts discussed in this report is the most active nanocatalyst. The only product of this reaction is 2-*t*-butyl *p*-cresol with selectivity of 100% and *p*-cresol conversion is 70%. The possible mechanism for this reaction system was discussed based on the reaction results. The reaction mechanism proposed involves the interaction of phenoxide from phenol and the *tert*-butyl cation from isobutene on $Cu_{1-x}Co_xFe_2O_4$.

Keywords. *Tert*-butylation; $Cu_{1-x}Co_xFe_2O_4$; spinel nanostructures; nanocatalysis; acidity.

1. Introduction

The catalytic reaction of phenol and cresols with *tert*-butyl alcohol or isobutene as well as methyl-*tert*-butyl ether have important commercial applications because C-alkylated products such as mono-*tert*-butyl derivatives of *m*-cresol are the precursors for a number of commercially important antioxidants and light protection agents.[1,2] Alkylation of *p*-cresol with *tert*-butanol gives 2-*tert*-butyl-*p*-cresol (TBC) and 2,6-di-*tert*-butyl-*p*-cresol (2,6-DTBC), commercially known as butylated hydroxy toluene (BHT).[3] The alkylated phenol products are used as raw materials for the synthesis of a variety of resins, durable surface coatings, varnishes, wire enamels, printing inks, surface-active agents, rubber chemicals, antioxidants, fungicides and petroleum additives.[4,5] Disadvantages of these reactions such as poor selectivity, high capital cost, reactor corrosion, and formation of byproducts that were experienced in the conventional method could be overcome by using solid oxide acid–base catalysts.[6] Among various oxides, transition metal oxides based on iron oxide in combination with other metal oxides are found to be the most active and selective catalyst for ortho-alkylation. The reaction is sensitive to the acidic and basic properties of the catalysts, the mole ratio of reactants and the type of alkylating agent. These studies represented that there is always a competition between *O*- and *C*-alkylation and that acid–base properties of the catalyst played an important role in the product selectivity.[7]

Ferrites which have reversed spinel-type structure are found to be highly active toward many aromatic alkylation reactions such as phenol alkylation, aniline methylation, and pyridine methylation.[8–10] The catalytic effectiveness of these systems is due to the ability of the metallic ions to migrate between the sublattices without altering the structure, which makes the catalyst efficient for many organic transformation reactions. The $Cu_{1-x}Co_xFe_2O_4$ system was found to be highly active for phenol alkylation with different alkylating agents.[11] The prime attraction of this catalyst system is its high ortho products selectivity along with high phenol conversion. A good correlation was found between activity,

*For correspondence

in terms of phenol conversion and selectivity of various products for this reaction, and the acid–base properties of the catalysts.

2. Experimental

2.1 *Materials measurements*

All chemical reagents used in our experiments were of analytical grade and were used as received without further purification. XRD patterns were recorded by the X-ray diffractometer (Philips-PW1800). Fourier transmission infrared (FT-IR) spectra of the powders (as pellets in KBr) were recorded using a Fourier transmission infrared spectrometer (Spectrum One FT-IR Spectrometer, Perkin Elmer Instruments) in the range of 4000 cm^{1-}. Conversion of the reactants was determined by HPLC (Waters600). The particle size and external morphology of the fine calcined powders were characterized by scanning electron microscopy, SEM (Philips-XL30), Samples were coated with gold at 10 mA for 2 min prior to SEM analysis.

2.2 *Synthesis of nanocatalysts*

$Cu_{1-x}Co_xFe_2O_4$ nanoparticles were prepared via a hydrothermal process. CTAB (1 g) was dissolved in 35 ml of distilled water. Then 1 g $FeCl_3{\cdot}6H_2O$ was added to it and was stirred for 10 min (S1). Afterwards, appropriate amounts of $CuCl_2.2H_2O$ and $CoCl_2.6H_2O$ salts, given in table 1, were dissolved in distilled water (S2) and added by a burette into S1 (S3). An aqueous solution of NaOH (S4) was introduced dropwise into S3 solution. The addition of S4 was stopped at pH 10-11 where a black precipitate formed. The reaction mixture was stirred for half hour. After stirring, the same was transferred to an autoclave. This autoclave was kept in an oven and heated at 160°C for 72 h. The autoclave was allowed to cool down to room temperature by natural convection. The product was then washed several times with distilled water followed by drying at room temperature.

2.3 *Catalytic activity tests*

Tertiary butylation of *p*-cresol was carried out in a reflux system. 10 cc nitromethane as a solvent and various amounts of *p*-cresol, MTBE and $Cu_{1-x}Co_xFe_2O_4$ nanoparticles were used in several catalysis tests for investigation of effects of different molar ratio of starting materials and catalysis in product selectivity and *p*-cresol conversion. The reflux system was heated up to 100°C under magnetic stirring in an oil bath equipped with an automatic temperature control system. The reaction was monitored by TLC. When the reaction was completed, the mixture was filtered to separate the $Cu_{1-x}Co_xFe_2O_4$ catalyst. Afterwards, the solvent was removed to obtain the combined organic phases and finally products obtained by washing of organic phases with mixture of n-hexane ethyl acetate and ethyl acetate (5:1). All products were characterized on the basis of FT-IR and ^1H NMR spectral data and by comparing the spectra to those of authentic samples or reported data.

3. Results

3.1 *Characterization of $Cu_{1-x}Co_xFe_2O_4$ nanoparticles*

Figure 1 shows the indexed x-ray diffraction (XRD) patterns of $Cu_{1-x}Co_xFe_2O_4$ (x = 0.0, 0.5 and 1.0). Cu-rich catalyst ($x = 0$) exhibits a diffraction pattern attributed to cubic spinel phase and a considerable amount of CuO and Fe_2O_3. Substitution of Cu with Co increases the overall crystallinity of the spinel phase. XRD pattern of $CoFe_2O_4$ (figure 1a) shows the formation of single phase cubic structure with dominant peak corresponding to (311) reflection indicating that the crystallites are preferentially oriented along (311) plane. The breadth of the Bragg peak is a combination of both instrument and sample dependent effects. To decouple these contributions, it is necessary to collect a diffraction pattern from the line broadening of a standard material such as silicon to determine the instrumental broadening. The instrument corrected

Table 1. The amount of starting materials for preparing of $Cu_{1-x}Co_xFe_2O_4$(x = 0, 0.25, 0.50, 0.75 and 1) nanoparticles.

Entry	x	$Cu_{1-x}Co_xFe_2O_4$	$CoCl_2$(g)	$CuCl_2$(g)	$FeCl_3$(g)	CTAB(g)
1	0	$CuFe_2O_4$	0	0.32	1	1
2	0.25	$Cu_{0.75}Co_{0.25}Fe_2O_4$	0.11	0.24	1	1
3	0.5	$Cu_{0.5}Co_{0.5}Fe_2O_4$	0.22	0.16	1	1
4	0.75	$Cu_{0.25}Co_{0.75}Fe_2O_4$	0.33	0.079	1	1
5	1	$CoFe_2O_4$	0.44	0	1	1

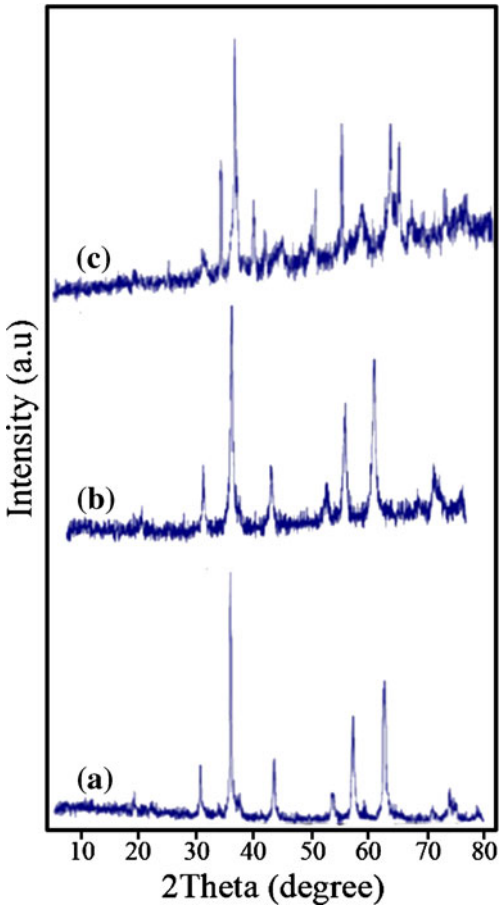

Figure 1. XRD patterns of (**a**) $CoFe_2O_4$, (**b**) $Cu_{0.5}Co_{0.5}Fe_2O_4$ and (**c**) $CuFe_2O_4$ nanoparticles.

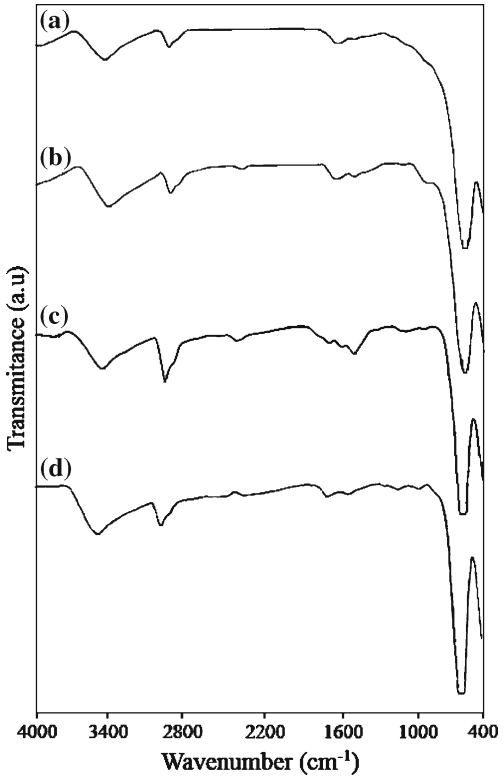

Figure 2. FT-IR spectra of (**a**) $CuFe_2O_4$, (**b**) $Co_{0.5}Cu_{0.5}Fe_2O_4$, (**c**) $Co_{0.75}Cu_{0.25}Fe_2O_4$ and (**d**) $CuFe_2O_4$ nanoparticles obtained by hydrothermal method.

broadening β corresponding to the diffraction peak of $Cu_{1-x}Co_xFe_2O_4$ (x = 0.0, 0.5 and 1.0) was estimated by using the below relation:

$$\beta = \beta_1 - \beta_2$$

The crystallite sizes (D_c) of $Cu_{1-x}Co_xFe_2O_4$ nanoparticles were calculated using the Debye–Scherrer equation (see table 2):

$$D_c = \frac{K\lambda}{\beta \cos\theta},$$

where β is the breadth of the observed diffraction line at its half-intensity maximum, K is the so-called shape factor, which usually takes a value of about 0.9, and λ is the wavelength of X-ray source used in XRD. X-ray powder diffraction data of $Cu_{1-x}Co_xFe_2O_4$ for most intense reflection are shown in table 2. As we can see from these data, crystallite sizes of $Cu_{1-x}Co_xFe_2O_4$ (x = 0.0, 0.5 and 1.0) calculated by Debye–Scherrer equation, are in the nanometer range.

Figure 2 shows FT-IR spectra of $Cu_{1-x}Co_xFe_2O_4$ nanoparticles. Two main broad metal–oxygen bands are observed in the FT-IR spectra of all spinels, and ferrites in particular. The highest one, ν_1, generally observed in the range of 600–550 cm^{-1}, corresponds to intrinsic stretching vibrations of the metal at the tetrahedral site, $M_{tetra} \leftrightarrow O$, whereas the lowest band, ν_2, usually observed in the range of 450–385 cm^{-1}, is assigned to octahedral metal stretching, $M_{octa} \leftrightarrow O$. However, no clear peak due to octahedrally coordinated metal ions has been observed due to

Table 2. X-ray powder diffraction data of $Cu_{1-x}Co_xFe_2O_4$ for most intense reflection.

Entry	X	$Cu_{1-x}Co_xFe_2O_4$	2θ(deg)	FWHM(deg)	D(nm)
1	0	$CuFe_2O_4$	35.4	0.24372	18
2	0.5	$Cu_{0.5}Co_{0.5}Fe_2O_4$	35.4	0.32946	22
3	1	$CoFe_2O_4$	35.2	0.32755	20

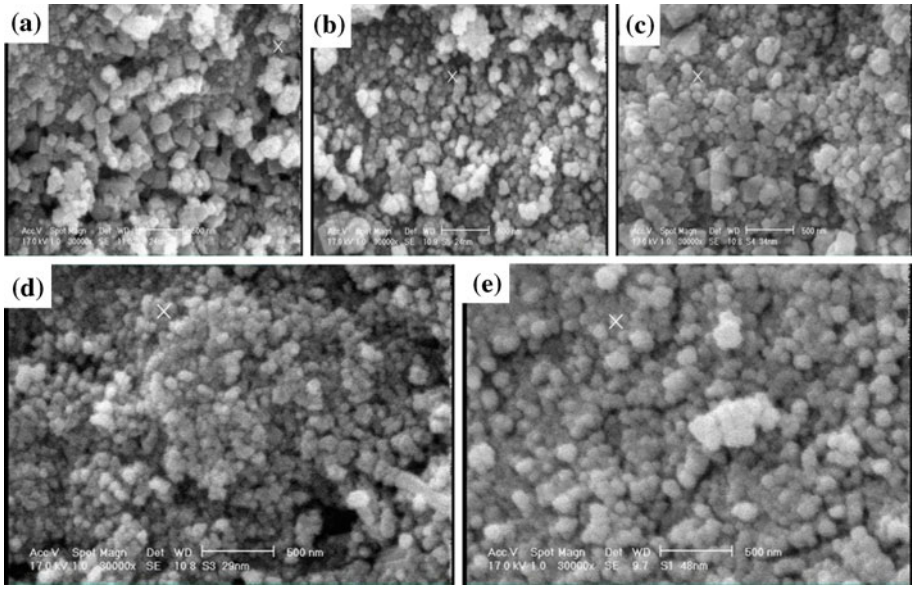

Figure 3. SEM images of $Cu_{1-x}Co_xFe_2O_4$ nanocatalysts: (**a**) $Cu_{0.5}Co_{0.5}Fe_2O_4$, (**b**) $Cu_{0.25}Co_{0.75}Fe_2O_4$, (**c**) $Cu_{0.75}Co_{0.25}Fe_2O_4$, (**d**) $CoFe_2O_4$ and (**e**) $CuFe_2O_4$.

the detection limit of our FT-IR instrument, which is expected to be below 400 cm^{-1}. The bands at 2923 and 2845 cm^{-1} are assigned to stretching of C–H group and the bands at 1120–1060 cm^{-1} to C–O stretching. The broad band centred at 3430 cm^{-1} can assigned to hydrogen bonded O–H stretching vibration arising from surface hydroxyl groups on nanoparticles. The absorption band at 1630 cm^{-1} on spectra refers to the vibration of remainder H_2O in the sample.

Surface morphology of the obtained $Cu_{1-x}Co_xFe_2O_4$ (x = 0, 0.25, 0.50, 0.75 and 1) nanoparticles was investigated by scanning electron microscopy (SEM) images. SEM micrographs were used to see the grain micro-structure of the nanoparticles, which would provide a better view of the grain development and grain sizes. SEM micrographs of $Cu_{1-x}Co_xFe_2O_4$ (x = 0, 0.25, 0.50, 0.75 and 1) are shown in figure 3. From the micrographs, it is clear that the grains also have different morphologies other than spherical. A broad size distribution is observed, which consists of nearly octahedral crystals with an average size of about 30 nm. The grain sizes measured of $Cu_{1-x}Co_xFe_2O_4$ (x = 0, 0.25, 0.50, 0.75 and 1) are 48, 34, 24, 24 and 29 nm, respectively.

3.2 *Catalytic activity studies*

3.2a *The effect of reaction time on tert-butylation of p-cresol*: Tertiary butylation of *p*-cresol with MTBE is a typical acid-catalyzed reaction. Alkylation of *p*-cresol with MTBE using spinel nanostructures gave a mixture of the isomers of tertbutylated phenols in terms of alkyls and the position of alkyl substituent. Only C-alkylated products can be formed depending on the reaction conditions such as the reaction temperature and the amount of MTBE, etc. The alkylation of *p*-cresol with MTBE using spinel nanostructures gives a mixture of TBC and 2,6-DTBC. With increasing

Table 3. Influence of catalyst composition on *p*-cresol conversion and products selectivity over $Cu_{1-x}Co_xFe_2O_4$ (x = 0, 0.25, 0.50, 0.75 and 1).

Entry	$Cu_{1-x}Co_xFe_2O_4$	*p*-cresol conversion (%)	TBC selectivity (%)	DTBC selectivity (%)
1	$CuFe_2O_4$	55	90	10
2	$Cu_{0.75}Co_{0.25}Fe_2O_4$	60	80	10
3	$Cu_{0.5}Co_{0.5}Fe_2O_4$	70	100	0
4	$Cu_{0.25}Co_{0.75}Fe_2O_4$	40	85	15
5	$CoFe_2O_4$	30	80	20

MTBE: *p*-cresol: catalyst mole ratio of 2:1:0.8, 100°C, CH_3NO_2 solvent and 6.5 h

Table 4. Influence of *tert*-butylation agent on *p*-cresol conversion and products selectivity over $Cu_{0.5}Co_{0.5}Fe_2O_4$.

Entry	*t*-butylating agent	*p*-cresol conversion (%)	TBC selectivity (%)	DTBC selectivity (%)
1	TBA	30	5	95
2	MTBE	70	0	100

t-butylating agent: *p*-cresol: catalyst mole ratio of 2:1:0.6, 100°C, CH_3NO_2 solvent and 6.5 h

reaction time, the conversion of *p*-cresol and the selectivity to TBC increase rapidly and reach an equilibrium level after 6.5 h, while the selectivity for 2,6-DTBC decreases rapidly and disappears gradually. The conversion of *p*-cresol reaches to 70% and the selectivity to TBC reaches to about 100% after 6.5 h. The increase in the selectivity to TBC is at the cost of a decrease in the selectivity to DTBC. The possible reason is that DTBC is converted into TBC. Thus, the best reaction time is 6.5 h because the catalyst activity has attained a stable higher activity state.

3.2b *The effect of catalyst composition on tert-butylation of p-cresol*: Table 3 illustrates the catalyst composition dependence of *p*-cresol conversion and selectivity of tertiary butylated *p*-cresol on $Cu_{1-x}Co_xFe_2O_4$ using MTBE as *tert*-butylating agent at 100°C with *tert*-butylating agent: *p*-cresol: catalyst mole ratio of 2:1:0.8, CH_3NO_2 solvent and 6.5 h. The important observations are: (i) *p*-cresol conversion increases from $x = 0$ to 0.5 and then decreases with further increase in x. (ii) 2-TBC selectivity decreases as Cu content decreases. (iii) $x = 0.5$ is associated with maximum *p*-cresol conversion and high selectivity towards 2-TBC formation. These results show that for achieving the maximum amount of catalytic activity, an optimum distribution between Cu atoms and neighboring heteroatoms (Co atoms) is needed.[7] We can easily find this optimum distribution when $x = 0.5$. Besides, low conversion of *p*-cresol in $x \geq 0.75$ may be due to de-*tert*-butylation of *tert*-butylated products in the presence of strong acidic sites. (Based on table 8 $x = 1$ has a maximum acidity and $x = 0$ has a maximum basic activity.)

3.2c *The effect of alkylation agent on tert-butylation of p-cresol*: For evaluation of the effect of *tert*-butylating agent in the conversion of *p*-cresol and selectivity of various products in the presence of $Cu_{1-x}Co_xFe_2O_4$ ($x = 0.5$) as a catalyst, two tests were carried out: in the first test, MBTE was used as a *tert*-butylating agent and in the other test, *tert*-butyl alcohol (TBA) was a *tert*-butylating agent. Results of these tests are summarized in table 4. These results clearly show that in tertiary butylation of *p*-cresol, MTBE as a *tert*-butylating agent is a far better choice than TBA. The possible reason is that by using TBA, H_2O is formed in the reaction media which may be absorbed by the acidic sites of catalyst and thus blocking the acidic sites of the catalyst. Consequently, the reaction on the surface of the catalyst is decreased. Besides, the etheric bond is weaker than alcoholic bond and therefore, carbocation is formed easily by MBTE than TBA.

3.2d *The effect of the amounts of $Cu_{0.5}Co_{0.5}Fe_2O_4$ nanoparticles on tert-butylation of p-cresol*: The influence of the molar ratio of $Cu_{0.5}Co_{0.5}Fe_2O_4$ to *p*-cresol on the conversion of *p*-cresol and the selectivity to TBC is shown in table 5. As the molar ratio of the nanocatalyst to *p*-cresol increases, both the conversion of *p*-cresol and the selectivity to TBC first increase and then decrease. The selectivity to 2,6-DTBC almost remains constant. This is attributed to the proportional increase in the amount of catalysts and the increase of acidity in the reaction system, which leads to increase in *p*-cresol conversion. However, a strong acid system does not lead to further alkylation of TBC with

Table 5. Influence of catalyst amount on *p*-cresol conversion and products selectivity over $Cu_{0.5}Co_{0.5}Fe_2O_4$.

Entry	Catalyst (g)	*p*-cresol conversion (%)	TBC selectivity (%)	DTBC selectivity (%)
1	0.1	40	100	0
2	0.15	70	100	0
3	0.2	60	100	0

MTBE: *p*-cresol = 2:1, 100°C, solvent: CH_3NO_2 and 6.5 h

Table 6. Influence of reaction temperature on *p*-cresol conversion and products selectivity over $Cu_{0.5}Co_{0.5}Fe_2O_4$.

Entry	Temperature (°C)	*p*-cresol conversion (%)	TBC selectivity (%)	DTBC selectivity (%)
1	100	70	100	0
2	70	50	95	5
3	45	20	95	5
4	R.T	0	0	0

MTBE: *p*-cresol: catalyst mole ratio of 2:1:0.6, CH_3NO_2 solvent and 6.5 h

MTBE. Considering both the conversion of *p*-cresol and the selectivity to TBC, the optimum molar ratio of $Cu_{0.5}Co_{0.5}Fe_2O_4$ to *p*-cresol is 1:1.

3.2e *The effect of the reaction temperature in the tert-butylation of p-cresol*: The influence of the reaction temperature on the conversion of *p*-cresol and the selectivity to TBC is shown in table 6. The conversion of *p*-cresol and the selectivity to TBC reach maxima at 100°C. With an increase in the temperature, the conversion of *p*-cresol and the selectivity to TBC first increased and then rapidly reached a steady state. The conversion of *p*-cresol increases from 0 to 70 mol% as the temperature changes from RT to 100°C. 2,4-DTBC selectivity also remains the same from 45 to 70°C, except at 100°C. It also indicates that lower temperature favours the formation of 2,6-DTBC, while higher temperature favours the formation of TBC. Considering both the conversion of *p*-cresol and the product distribution, the optimum reaction temperature should be around 100°C. At this temperature, both the selectivity to TBC and the conversion of *p*-cresol reach the highest value. These results indicate that no 2,6-DTBC in the 100°C may be due to de-*tert*-butylation reactions at higher temperature. However, for the precise investigation of the effect of temperature in *tert*-butylation reactions, we have carried out the kinetic investigation of these reactions in parallel to the work which is presented in this report, but because of high volume of kinetic investigation of this research, we are collecting our data to report as a separate paper.

3.2f *The effect of the molar ratio of MTBE to p-cresol in tert-butylation of p-cresol*: The influence of the molar ratio of MTBE to *p*-cresol on the conversion of *p*-cresol and the selectivity to TBC in *tert*-butylation using $Cu_{0.5}Co_{0.5}Fe_2O_4$ are shown in table 7. As the molar ratio of MTBE to *p*-cresol increases, the conversion of *p*-cresol and the selectivity to TBC first increase and then rapidly reach to a steady state, while the selectivity for 2,6-DTBC is zero. Both high conversion of *p*-cresol and the selectivity to TBC are achieved when the molar ratio of *p*-cresol to MTBE is 1:2.

4. Discussion

4.1 *Catalytic performance*

From the activity data, it is evident that Cu-rich samples are active catalysts for tertiary butylation and Co-dominant compositions show poor activity, emphasizing the important role of Cu in this reaction. However, the equal bulk contents of Cu and Co at $x = 0.5$ show maximum activity. Except at $x = 0.5$, *p*-cresol conversion is between 30 and 60 mol% for all other compositions, suggesting that tertiary butylation activity is mainly due to the Cu + Co combination, of which Cu is the highly active. An important aspect of the butylation reaction is related to product selectivity too. At an optimum temperature of 100°C, MTBE attaches to the phenolic ring to give tertbutyl phenols. Unlike lower alkylations, tertiary butylation of *p*-cresol gives two products, namely, 2-TBC and 2,6-DTBC, and the selectivity of each product depends on the various reaction parameters.

Table 7. Influence of MTBE: *p*-cresol mole ratio on *p*-cresol and product selectivity over $Cu_{0.5}Co_{0.5}Fe_2O_4$.

Entry	MTBE: *p*-cresol	*p*-cresol conversion (%)	TBC selectivity (%)	DTBC selectivity (%)
1	2:1	70	100	0
2	1.5:1	40	100	0
3	1:1	20	100	0

p-cresol: catalyst mole ratio of 1:0.6, 100°C, CH_3NO_2 solvent and 6.5 h

Table 8. Textural and acid-base characteristic of $Cu_{1-x}Co_xFe_2O_4$ 10.

Entry	X	a(A°)	S_{BET} (m^2/g)	Pore volume (cc/g)(10^{-2})	Relative acidity(basicity)[a]
1	0	8.3898	28.8	5.1	300 (580)
2	0.25	8.4051	34.0	6.7	381 (510)
3	0.50	8.4012	43.8	10.9	497 (420)
4	0.75	8.3982	36.6	6.4	623 (275)
5	1.0	8.3998	36.8	5.9	782 (210)

[a]Obtained from FT-IR studies of pyridine and CO_2 adsorbed catalysts [23]

4.2 *Reaction mechanism*

A detailed investigation of the acid–base properties of the $Cu_{1-x}Co_xFe_2O_4$ catalyst system was carried out by Mathew *et al.*[12] The acidic and textural properties of $Cu_{1-x}Co_xFe_2O_4$ which well obtained by Mathew research group are summarized in table 8. Our catalytic results and their investigation about $Cu_{1-x}Co_xFe_2O_4$ acidic properties are in good agreement. Based on their investigations and our results, four important points which help in understanding of tertiary butylation activity are: (i) the $Cu_{1-x}Co_xFe_2O_4$ surface is dominated by Lewis acid character (ii) a relatively weak acidic character at x = 0 increases with Co content to highly acidic character at x = 1.0 and an increase in number and strength of acidic sites (iii) the basic character of the catalyst decreases with increasing x. (iv) the acid–base character on the catalyst surface is predominantly due to octahedral cations, and the Lewis acidity changes significantly depending on the easily reducible (Cu^{2+}) or nonreducible (Co^{2+}) ions in the neighbourhood. Generally, robust Co^{2+} in the neighbourhood increases the acidity. A simple comparison of *p*-cresol conversion and acid–base character demonstrates that neither strong acidic nor strong basic character helps the tertiary butylation reaction. It is also evident that the intermediate acid–base character observed for the x = 0.5 composition with high catalytic activity indicates an optimum level of acid–base sites are required for better catalytic performance in terms of *p*-cresol conversion and overall product yield. In accordance to the above discussion, we proposed a mechanism which is summarized in the figure 4.

Alkylation of *p*-cresol, just like other aromatic compounds, follows the Friedel-Craft mechanism. From electrophilic substitution it is clear that the *tert*-butyl cation attacks the *p*-cresol ring preferentially in ortho positions to the –OH group. The ratio of isomers formed initially is kinetically controlled and is determined by phenolic OH groups and incoming *tert*-butyl cations in

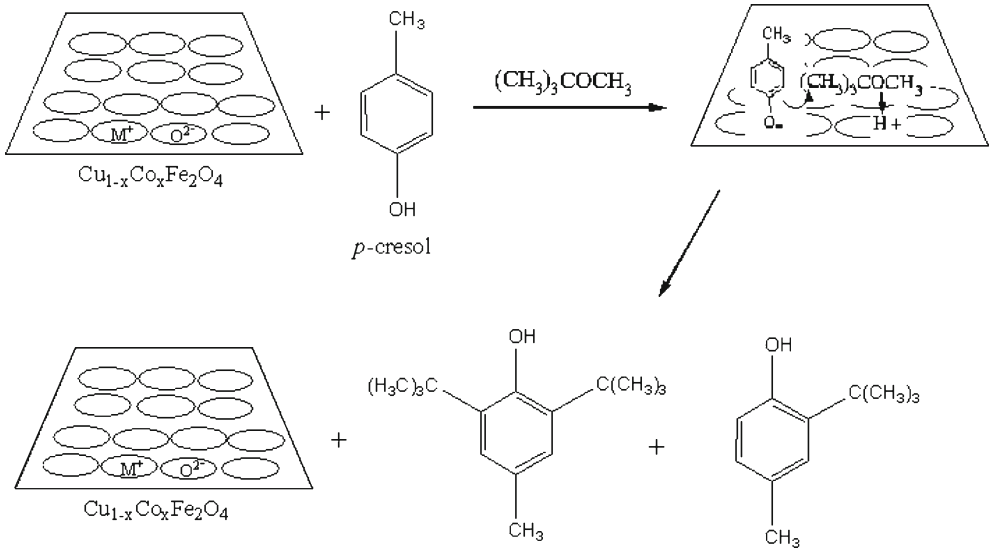

Figure 4. Schematic diagram of the proposed mechanism of tertiary butylation of *p*-cresol by $Cu_{1-x}Co_xFe_2O_4$ nanocatalysts.

the present case. Though the mono-*tert*-butylated *p*-cresol are more active than *p*-cresol, subsequent tertiary butylation occurs only when there is less steric hindrance.[12]

5. Conclusion

In this research, $Cu_{1-x}Co_xFe_2O_4$ (x = 0, 0.25, 0.50, 0.75 and 1) spinel nanostructures were synthesized and characterized, and their catalytic activity in the *tert*-butylation of *p*-cresol were examined. Under optimal reaction conditions, more than 70% conversion of *p*-cresol and about 100% selectivity to TBC were obtained. The catalysts can be recycled after the reaction. In comparison with the solid acid catalysts, the *tert*-butylation of *p*-cresol using spinel nanostrucures can be conducted at mild reaction conditions. It is concluded that the $Cu_{0.5}Co_{0.5}Fe_2O_4$ nanoparticles have strong acidic nature and can be used as a substitute for traditional acids.

References

1. Chhabra J S, Athar J, Agranal J P and Singh H 1993 *Rubber Compos. Process. Appl.* **20** 305
2. Ajit S, Nilesh S and Shriniwas S 2004 *Appl. Catal. A: Gen.* **267** 5
3. Karthik M, Vinu A and Tripathi K N 2005 *Micropor. Mater.* **70** 207
4. Gonzalez V 1981 *Rubber Chem. Technol.* **54** 134
5. Emil D and Vasile H 2003 *J. Catal.* **218** 249
6. Fiege H 2000 *Ullmann's Encyclopedia of Industrial Chemistry*; Federal Republic of Germany, Bayer A G, Leverkusen, A19, p. 324
7. Thomas M, Bollapragada S R and Chinnakonda S G 2004 *J. Catal.* **222** 107
8. Rajgopal R, Vetrivel R and Rao B S 2000 *Catal. Lett.* **65** 99
9. Rao B S, Sreekumar K and Jyothi T M 1998 *Indian Patent* 2707/98
10. Sreekumar K, Jyothi T M, Mathew T, Talawar M B, Sugunan S and Rao B S 2000 *J. Mol. Catal. A* **159** 327
11. Mathew T, Shylesh S, Devassy M B and Vijayaraj M 2004 *Appl. Catal. A: Gen.* **273** 35
12. Mathew T, Vijayaraj M, Pai S, Tope B B, Hegde G S, Rao S B and Gopinath S C 2004 *J. Catal.* **227** 175